Retrieval of Ice Cloud Parameters Using the Advanced Microwave Sounding Unit

LIMIN ZHAO

QSS Group, Inc., Lanham, Maryland

FUZHONG WENG

NOAA/NESDIS/Office of Research and Applications, Camp Springs, Maryland

(Manuscript received 20 March 2001, in final form 16 September 2001)

ABSTRACT

An algorithm is developed to derive cloud ice water path (IWP) and ice particle effective diameters D_e from the advanced microwave sounding unit (AMSU) measurements. In the algorithm, both IWP and D_e are related to the ice particle scattering parameters, which are determined from the AMSU 89- and 150-GHz measurements. The ratio of the scattering parameters measured at two frequencies provides a direct estimate of D_e. IWP is then derived from the scattering parameter at 150 GHz with the derived D_e and the constant bulk volume density. A screening procedure is developed to discriminate the scattering signatures between atmospheric clouds and surface materials. The major error sources affecting the retrievals are identified. The errors of retrieved effective diameter are primarily controlled by the errors in estimating cloud-base brightness temperatures at 89 and 150 GHz and the errors of the bulk volume density. It is shown that D_e possibly contains an error of 5%–20%. For the retrieval of cloud ice water path, the errors are influenced by the uncertainties in estimated cloud-base brightness temperature, retrieved particle effective diameter, and particle volume density. A 30% error in bulk volume would alone result in a 25% error in retrieved IWP. The algorithm is applied for various weather events and can primarily detect the precipitating ice clouds as well as thick nonprecipitating clouds because of an increasing sensitivity of AMSU measurements at 150 GHz to smaller particle sizes. These results demonstrate the use of 89- and 150-GHz channels for studying the ice cloud properties and their spatial variability under various atmospheric environments.

1. Introduction

The distribution of microphysical parameters, such as ice water content and particle diameters, is a key requirement for characterizing ice clouds and their influence on the climate. For example, the reflection of shortwave radiation by ice clouds reduces the solar energy reaching the earth's surface. On the other hand, ice clouds can trap the longwave radiation emitted from the surface, resulting in less radiation to space in comparison with clear-sky conditions. The net radiative flux at the earth's surface that results from the above two processes, however, depends on accurate description of the ice cloud parameters for radiative transfer calculations in climate models (Stephens and Webster 1981; Liou 1986). Therefore, a quantitative measurement of microphysical parameters in ice clouds is important both for the validation of global climate models and for understanding the nature variability of the earth's climate (Heymsfield and Donner 1990; Ebert and Curry 1992; Fu and Liou 1993).

Because of the scattering effects of ice clouds, satellite microwave measurements provide more direct estimates of ice water path IWP (or vertically integrated ice water content) in comparison with the existing visible and infrared techniques (Rossow and Shiffer 1991; Minnis et al. 1993). The scattering signatures from ice clouds can be used also to estimate surface rainfall rate (Spencer et al. 1983; Adler et al. 1993; Grody 1991). Evans and Stephens (1995a,b) theoretically demonstrated the feasibility of retrieving ice water path in thin cirrus clouds using millimeter-wavelength observations. It was shown that the sensitivity of brightness temperatures at higher frequencies to IWP is nearly independent of cloud temperature and the details of the underlying atmosphere because of the higher scattering albedo. Vivekanandan et al. (1991) studied the possibility of retrieving precipitation-sized ice water amount using simulated measurements at lower frequencies (e.g., 37 and 85 GHz). It was found that the brightness temperature monotonically decreases as the cloud optical thickness increases. However, the relationship is modulated by the changes of particle bulk volume density.

Corresponding author address: Fuzhong Weng, NOAA/NESDIS/Office of Research and Applications, 5200 Auth Road, Rm 601, Camp Springs, MD 20746.
E-mail: fuzhong.weng@noaa.gov

The retrieval algorithms were developed and tested recently using aircraft millimeter-wavelength measurements (Liu and Curry 1998, 1999; Weng and Grody 2000, hereinafter WG00). Liu and Curry (1998) presented a method to retrieve IWP using airborne millimeter-wave imaging radiometer (MIR) data at 89-, 150-, and 220-GHz channels. The algorithm was modified further to derive IWP in tropical cloud systems using the satellite microwave data (Liu and Curry 1999). Although the IWP algorithm works well for cirrus clouds in the Tropics, an uncertainty arises due to an unknown particle size. WG00 proposed an algorithm to derive both IWP and ice particle effective diameter (D_e) using dual millimeter-wavelength measurements. They found that, for a given particle bulk volume density, the brightness temperature at microwave frequencies can be uniquely related to IWP and D_e through a two-stream radiative transfer model solution. The algorithm was tested with the measurements obtained from MIR. The retrieved IWP and D_e display a reasonable spatial distribution comparable to the radar and infrared measurements. Methods to retrieve both ice water path and median particle size of the nonprecipitating cirrus clouds over tropical oceans were also recently proposed by Liu and Curry (2000) and Deeter and Evans (2000).

Most of these retrieval algorithms were tested using aircraft in situ measurements over the tropical ocean. The discrimination between atmospheric ice clouds and surface scatterers, such as desert sands and snow cover, was not previously discussed. The clear-sky or cloud-base temperature is also assumed in general to be constant (e.g., WG00). The purpose of this study is to develop an algorithm that is globally applicable for retrieving the ice particle size and water path. The physical approach described by WG00 is enhanced further and is made more suitable for satellite measurements.

This paper is organized as follows. Section 2 briefly describes the characteristics of the advanced microwave sounding unit (AMSU) instruments. Section 3 presents the retrieval algorithm, a method to estimate the upwelling brightness temperature at cloud bases, and a screening procedure to remove the surface scattering contaminations. Section 4 shows some retrieval results under various cloud systems. In addition, the relationships between the retrieved parameters (IWP, D_e) and other geophysical parameters such as cloud-top temperature, liquid water path, and rainfall rate are examined. In section 5, a comprehensive error analysis is performed to examine the effects of uncertainties in the instrument noise, cloud-base temperature, particle size distributions, and bulk volume density on the algorithm. A summary and concluding remarks are given in section 6.

2. AMSU instruments

The AMSU on the new generation National Oceanic and Atmospheric Administration (NOAA) polar-orbiting satellites, first placed into operation in May of 1998, contains both the ''A'' and ''B'' modules (Grody et al. 2001). The AMSU-A has 15 channels in the frequency range of 23–89 GHz with window channels at 23.8, 31.4, 50.3, and 89 GHz that are the primary channels used for the retrieval of surface hydrological products. The instrument has an instantaneous field of view (FOV) of 3.3° at the half-power points, which provides a spatial resolution of 48 km at nadir. There are a total of 30 measurements on each scan line. The AMSU-B contains five channels in the frequency range of 89–183 GHz. Its antenna has an instantaneous FOV of 1.1° at the half-power points, resulting in a spatial resolution of 16 km at nadir. There are total of 90 measurements on each scan line. Because the satellite is in a sun-synchronous orbit, the AMSU provides near-global observations 2 times per day.

Although the AMSU-B was designed primarily for profiling atmospheric water vapor, its window channels at 89 and 150 GHz also provide information on ice clouds because of their scattering characteristics. However, there were two notable problems in the first AMSU instrument on the *NOAA-15* satellite. First, the AMSU-A window channels exhibit asymmetric radiances along each scan line. This asymmetry adversely affects the quality of the cloud liquid water and total precipitable water products. The asymmetry fortunately is constant with time and can be corrected using a simple algorithm (Weng et al. 2000). The second problem is that the AMSU-B measurements at 150 and 183 $\pm$ 3 GHz initially were contaminated by radio frequency interference. This contamination was removed using the algorithm developed by the Met Office. These correction procedures have led to operational applications of AMSU data for generating many nonsounding products such as cloud liquid and water vapor with improved quality (Grody et al. 2001).

3. Methodology

a. Physical basis of retrieval algorithm

With a two-stream approximation at microwave frequencies, WG00 derived a relationship between the brightness temperature emanating from the ice clouds $T_B(z_t, \mu)$ and that at the cloud base $T_B(z_b, \mu)$ as

$$T_B(z_t, \mu) = \frac{T_B(z_b, \mu)}{1 + \Omega(\mu)}, \tag{1}$$

where z_t and z_b are the heights of the cloud top and base, respectively; μ is the cosine of the zenith angle; and Ω is the ice cloud scattering parameter. It is defined as

$$\Omega(\mu) = \frac{\kappa\tau}{2a} = \frac{1}{2\mu}(1 - \omega g)\tau, \tag{2}$$

where τ is the ice cloud optical thickness, κ is the eigenvalue, a is the similarity parameter, g is the asymmetry factor, and ω is the single-scattering albedo (refer to WG00 for more details).

The brightness temperature $T_B(z_t, \mu)$ in Eq. (1) decreases as the scattering parameter Ω increases. Variation of the scattering parameter results from the changes of the ice water path and particle size in ice clouds. Therefore, the influence of ice cloud microphysical parameters on microwave measurements can be quantitatively analyzed using Eqs. (1) and (2). In particular, the scattering parameter can be related to the cloud ice water path and particle size through the optical thickness, which is defined as

$$\tau = \int_{Z_b}^{Z_t} dz \int_0^\infty \frac{\pi}{4} D^2 Q_{\text{ext}}(x, m) N(D)\, dD, \qquad (3)$$

where Q_{ext} is the extinction efficiency of ice particles; $N(D)$ is the particle size distribution function; x is the size parameter ($x = \pi D/\lambda$); and m is the complex refractive index, which might vary with the ice particle bulk volume density. For spherical ice particles with the size distribution $N(D)$, IWP can be expressed as

$$\text{IWP} = \int_{Z_b}^{Z_t} dz \int_0^\infty \frac{\pi}{6} \rho_i D^3 N(D)\, dD, \qquad (4)$$

where ρ_i is the ice particle bulk volume density. For polydispersed ice particles, the scattering parameter can be expressed as a function of IWP and D_e through the manipulation of Eqs. (3) and (4); that is,

$$\Omega(\mu) = (\text{IWP}/\mu\rho_i D_e)\Omega_N(x, m), \qquad (5)$$

where Ω_N is the normalized scattering parameter defined as

$$\Omega_N = (3/4)(1 - \omega g)\, \overline{Q}_{\text{ext}}(x, m), \qquad (6)$$

and $\overline{Q}_{\text{ext}}$ is an averaged extinction efficiency of the ice particles weighted by the size distribution of $N(D)$; that is,

$$\overline{Q}_{\text{exl}}(x, m) = \frac{\int_0^\infty D^2 Q_{\text{ext}}(x, m) N(D)\, dD}{\int_0^\infty D^2 N(D)\, dD}. \qquad (7)$$

When the upwelling brightness temperature $T_B(z_b, \mu)$ at the cloud base is known, Ω can also be determined through Eq. (1) as

$$\Omega(\mu) = \frac{T_B(z_b, \mu) - T_B(z_t, \mu)}{T_B(z_t, \mu)}, \qquad (8)$$

where $T_B(z_t, \mu)$, the upwelling brightness temperature at the cloud top, is a direct measurement from satellites. Equation (5) can be used to derive the cloud ice water path when rearranged:

$$\text{IWP} = \mu D_e \rho_i (\Omega/\Omega_N), \qquad (9)$$

As shown in Eq. (9), IWP is directly proportional to Ω. However, the relationship between Ω_N and D_e is nonlinear and may depend on the particular ice particle size distribution and bulk volume density. Therefore, measurements at two distinct frequencies normally are required to determine unambiguously both IWP and D_e for a given particle bulk volume density (Evans and Stephens 1995a,b; WG00). Provided that the bulk volume density of ice particles can be determined from other sources independently (i.e., assumed to be either a constant or a function of ice particle size), the IWP essentially only depend on the scattering parameter Ω and D_e. Because most published bulk density-size relations are derived for ice particles in nonprecipitating cirrus clouds, there are some uncertainties in using these relationships in the retrieval because the AMSU measurements are primarily sensitive to the precipitating ice clouds. Thus, a constant density of 600 kg m^{-3} is used in this study. The retrieval errors due to the uncertainties of bulk volume density are studied and presented in section 5.

b. The IWP and D_e retrieval algorithms

The scattering parameter ratio of two channels is defined and used here to determine D_e by eliminating IWP; that is,

$$r(D_e) = \frac{\Omega_{89}}{\Omega_{150}} = \frac{\Omega_{N89}(x, m)}{\Omega_{N150}(x, m)}. \qquad (10)$$

Note that the scattering parameter ratio ideally varies between 0 and 1. For ice clouds having small ice particles, Ω_{89} nearly vanishes and the ratio approaches 0. For ice particles having a larger effective diameter, the scattering parameter ratio approaches unity when the scattering intensities at 89 and 150 GHz reach their geometrical optical limit.

An empirical relationship between r and D_e is derived using simulated data from a radiative transfer model (Weng 1992). The Mie theory is applied to determine the scattering and absorption properties of the ice particles at 89 and 150 GHz. In the simulation, cloud ice water content is randomly generated within a range of 0–0.5 g m^{-3}, and the cloud ice particles are assumed to be spherical and distributed using the modified gamma distribution with an exponent of 2 (Ulbrich 1983). The ice cloud base is at 9 km with its thickness of 1 km, which simulated a general atmosphere condition for ice clouds. The effective particle diameter randomly varies within a range of 0.1–3.5 mm. The incident radiation at the cloud base is set to a constant value corresponding to a brightness temperature of 280 K. Cumming's mixing formula is used to compute the refractive index of ice–air mixture (Cumming 1952). The simulations were made with various combinations of D_e and N_0 (a total of 62 500 gamma size distribution) and the results are shown in Fig. 1. Note that the ratio initially increases as D_e increases and then approaches to a constant when ice particle effective sizes become very large. For small D_e($<$0.4 mm), the scattering parameter of 89 GHz is small because of its lack of sensitivity to

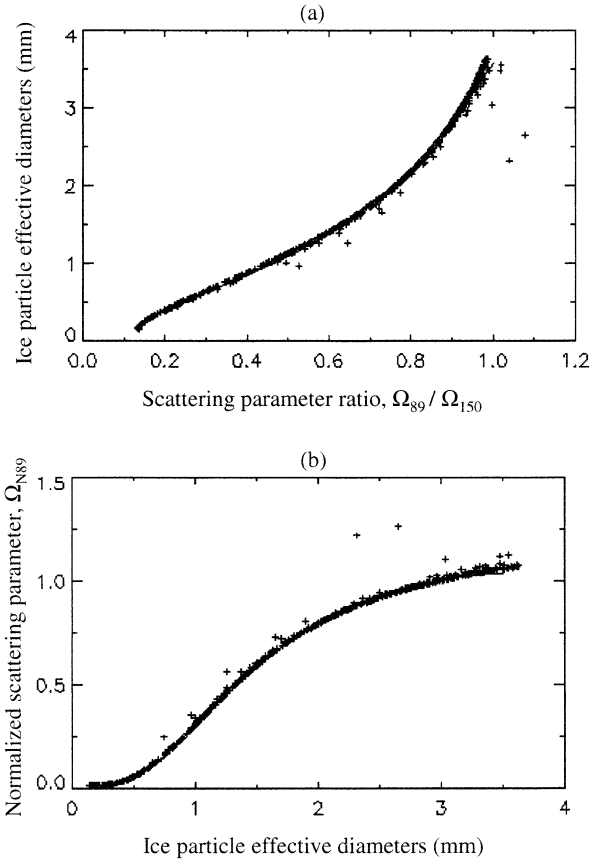

FIG. 1. (a) Relationships between particle effective diameter and the scattering parameter ratio. (b) The relationship between normalized scattering parameter and particle effective diameter.

the small-size ice particles. Therefore, the size information cannot be determined uniquely by the scattering parameter ratio of 89 and 150 GHz. A higher-frequency pair (i.e., 150 and 220 GHz) is required for detecting these small-size ice particles (Evans et al. 1998). For D_e between 0.4 and 2.5 mm, Ω_N at both 89 and 150 GHz linearly increases with D_e, and Ω_N at 150 GHz is much higher than that at 89 GHz. However, for a larger D_e (greater than 3.5 mm), Ω_N at both frequencies tends to approach to the same constant value. The minimum detectable ice particle size is about 0.5 mm for 89 GHz. With the dual-frequency measurements at 89 and 150 GHz, reliable results are expected when the ratio ranges from 0.2 to 0.8.

The regression relations of D_e–r and Ω_N–D_e are obtained from data in Fig. 1 as follows:

$$D_e = a_0 + a_1 r + a_2 r^2 + a_3 r^3 \quad \text{and} \tag{11}$$

$$\Omega_{N89 \text{ or } 150} = \exp\{b_0 + b_1 \ln(D_e) + b_2[\ln(D_e)]^2\}, \tag{12}$$

where a_i ($i = 0$, 1, 2, and 3) and b_i ($i = 0$, 1, and 2) are the regression coefficients that may be dependent on the ice particle bulk volume density and assumed size distribution. Table 1 gives the coefficients used in this study.

TABLE 1. The coefficients used in the IWP and D_e algorithms.

D_e	a_0	a_1	a_2	a_3
	−0.248 43	3.867 26	−4.707 82	4.671 50
		b_0	b_1	b_2
IWP	$D_e < 1.2$ mm	−1.746 63	1.907 11	−0.730 29
	$D_e \geq 1.2$ mm	−1.585 71	1.522 30	1.522 30

When the brightness temperatures at ice cloud base are estimated, the scattering parameter ratio can be computed using Eq. (9) with satellite measurements from two frequencies. Thus, IWP and D_e can be determined unambiguously from Eqs. (11), (12), and (9) for a given bulk volume density. The method to estimate the cloud base temperatures is given below.

c. Estimating the upwelling brightness temperatures at ice cloud bases

For a scatter-free, isothermal atmosphere, brightness temperatures at microwave frequencies may be approximated as (Weng and Grody 1998)

$$T_B = T_s[1 - (1 - \varepsilon)\Im^2] - \Delta T(1 - \Im)[1 + (1 - \varepsilon)\Im], \tag{13}$$

where $\Im$ is atmospheric transmittance, ε is the surface emissivity, T_s is the surface temperature, and ΔT is the temperature difference between the surface and the atmospheric mean temperature. The atmospheric transmittance can be further expressed as

$$\Im = \exp[-(\tau_o + \tau_v + \tau_l)/\mu], \tag{14}$$

where τ_o, τ_v, and τ_l are the optical thickness of oxygen, water vapor, and cloud liquid water, respectively. It was pointed out that the brightness temperature estimated with Eq. (13) contains less than 2% of errors. Thus, the brightness temperatures of 89 and 150 GHz at ice cloud bases $T_B(z_b, \mu)$ can be estimated using Eq. (13) with AMSU measurements at lower frequencies. However, the assumption was made that the brightness temperatures at lower frequencies are not affected by the presence of ice clouds.

Note that the emissivity in Eq. (13) is a function of the surface temperature, wind speed, and salinity over oceans and is computed using a previously developed model (Klein and Swift 1977; Stogryn 1972; Holinger 1971). Here, τ_v is parameterized as a function of water vapor path, and τ_l is derived as a function of cloud liquid water and cloud layer temperature. In addition, τ_o is parameterized as a function of surface temperature (Weng et al. 2000). Over oceans, the cloud liquid water and water vapor path can be retrieved directly from the AMSU lower frequencies (Grody et al. 2001), whereas surface wind and temperature are obtained from the Na-

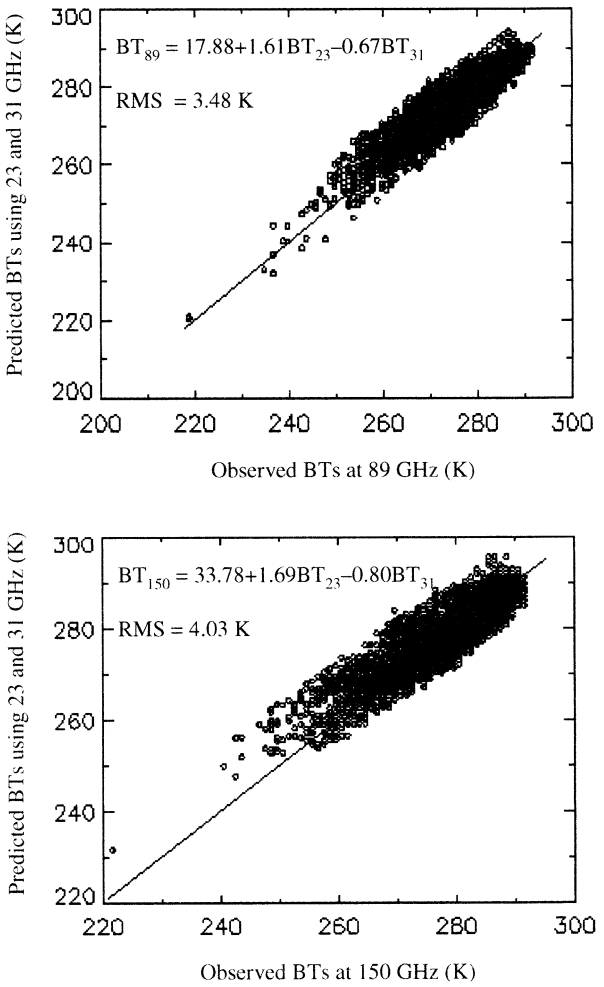

FIG. 2. Regression relationship derived to estimate cloud-base brightness temperatures at (top) 89 and (bottom) 150 GHz using the measurements at 23 and 31 GHz.

tional Centers for Environmental Prediction (NCEP) global data assimilation system (GDAS).

Over land, the cloud-base brightness temperature is estimated using an empirical relationship between the AMSU lower and higher frequencies. In doing so, the AMSU brightness temperatures are collected under the scatter-free conditions and are then used to derive the relationships. The AMSU clear radiances are identified using infrared data from the advanced very high resolution radiometer (AVHRR) and surface temperature. The AVHRR is also on *NOAA-15* and *NOAA-16* satellites. The AMSU measurements corresponding to IR temperatures less than 275 K are excluded from the collocated data because the data possibly contain ice clouds (Stowe et al. 1999). The AMSU collocation data are also limited to within $\pm 45°$ of scan angles to eliminate the effects of large footprints. As shown in Fig. 2, the brightness temperatures of 89 and 150 GHz at the ice cloud bases can be estimated with an rms error of about 4.0 K that is equivalent to the results over oceans. This result implies that the brightness temperature depressions at 89 and 150 GHz due to clouds must be greater than 4.0 K so that the clouds can be identified reliably. This rms error corresponds to minimum thresholds of 0.01 and 0.02 for the scattering parameters at 89 and 150 GHz, respectively.

d. A screening procedure

The scattering signatures resulting from desert, sea ice, and snow particles at higher microwave frequencies are similar to that of the ice particles because the dielectric constants among these scatters are almost the same. Therefore, for global application of the IWP and D_e retrieval algorithm, a procedure is developed to discriminate the scattering signatures between atmospheres and various surface materials. The AMSU alone provides very limited information on surface types, however, because of its lack of polarization measurements. Other datasets such as AVHRR infrared and GDAS surface temperature and surface types are used as part of the proposed screening procedure.

Surface scattering from snow and sea ice can be largely removed using the measurements at lower AMSU-A frequencies. AMSU-A-derived products of snow cover and sea-ice concentration are first used to indicate their presence. The GDAS surface temperature T_s less than 269 K is used as an additional threshold to identify the scattering signatures of frozen surfaces. The retrieval of atmospheric ice is not performed under these surface conditions. Furthermore, there is no retrieval over high terrains such as the Tibetan Plateau where the surface temperatures usually are less than 273 K.

Deserts also scatter at AMSU 89 and 150 GHz (Weng et al. 2001). The scattering from the clouds can be easily separated from the surface using the satellite infrared measurements and GDAS surface temperatures, however. If the atmosphere is free from ice clouds, then the IR temperature is close to the surface temperature, and therefore the scattering at 89 and 150 GHz must result from the surface. More specific, for desert scatterers, the temperature difference is less than 10 K and Ω is greater than 0.01. In case the satellite infrared data are not available, AMSU measurements at 183 ± 7 GHz can be used as a substitute because the channel peaks in the lower troposphere and is less affected by the surface (Wang et al. 1997). In fact, for the *NOAA-15* satellite, the infrared channels from AVHRR failed soon after its launch. As a result, the operational IWP and D_e algorithm is implemented without use of IR measurements. The global IWP and D_e retrieval algorithm, including the entire screening procedure, is summarized in Fig. 3. Note that the upwelling brightness temperatures at 89 and 150 GHz are corrected to the two-stream brightness temperatures before they are used in the retrieval.

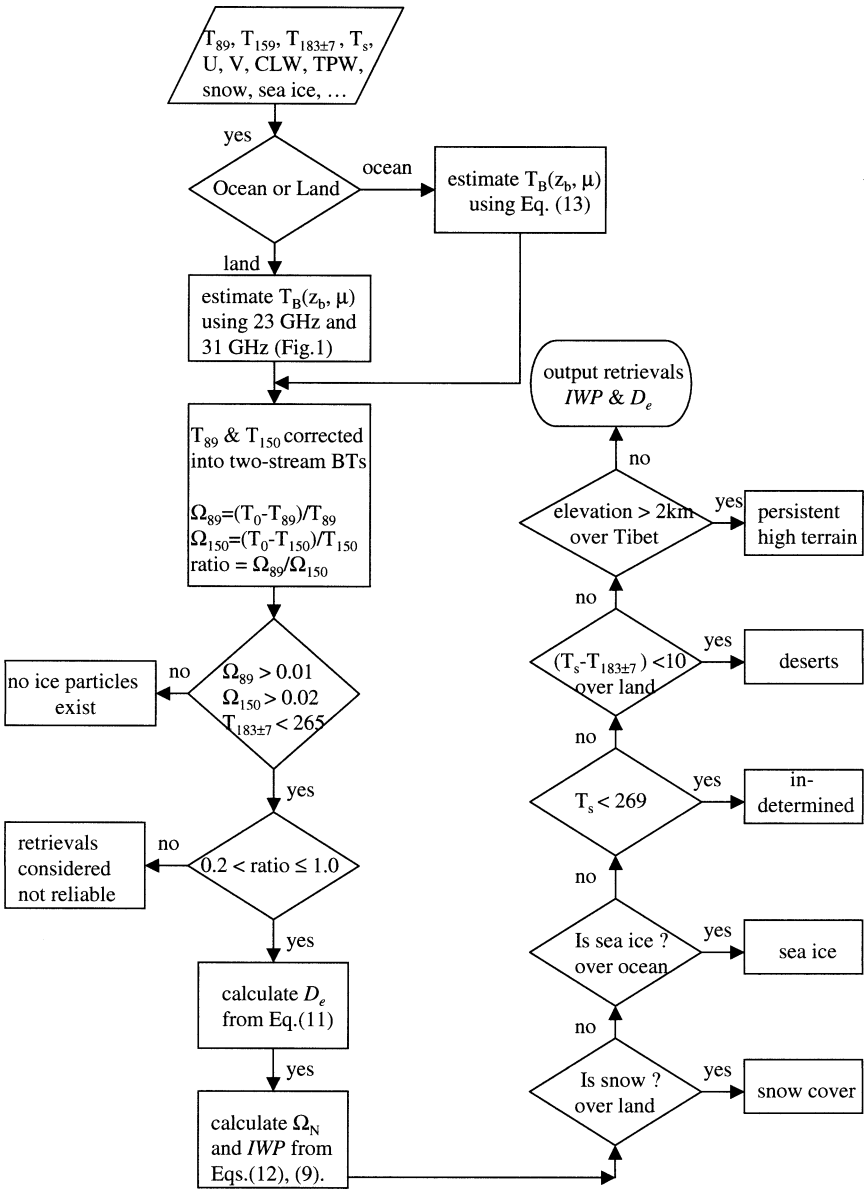

FIG. 3. The AMSU algorithm for retrieving ice cloud parameters.

4. Results and discussions

a. A midlatitude winter storm

Figure 4a displays the distribution of the multisensor surface hourly rainfall, which is an optimum composite product of radar and rain gauge observations (Seo 1998) from NCEP, for a winter storm occurring on 23 November 1999. Figure 4b shows the AMSU brightness temperature measurements at different frequencies along a line that crosses through the center of the storm (32°N, 96.75°W). It can be seen that the maximum brightness temperature depression occurs at 150 GHz. The temperature depression at 23 and 31 GHz is less than 10 K, as compared with more than 70 K at 89 and 150 GHz. These structures indicate the presence of a large number of frozen hydrometeors. Figure 4c shows the variations of scattering parameters at 89 and 150 GHz. As expected, 150 GHz is more sensitive to ice particles and has a larger scattering parameter in comparison with 89 GHz. Figure 4d displays the cloud-top temperature estimated from AVHRR 12-μm IR data. It can be seen that colder cloud-top temperatures generally result in large brightness temperature depressions. As shown in Figs. 4e,f, the retrieved IWP and D_e agree well with the surface rainfall features, especially near the convective region. Large ice particles and IWP appear near the center of the storm and produce a large amount of rainfall reported at surface. However, the location of the maximum of IWP does not correspond to that of the surface maximum rainfall. This dislocation may be

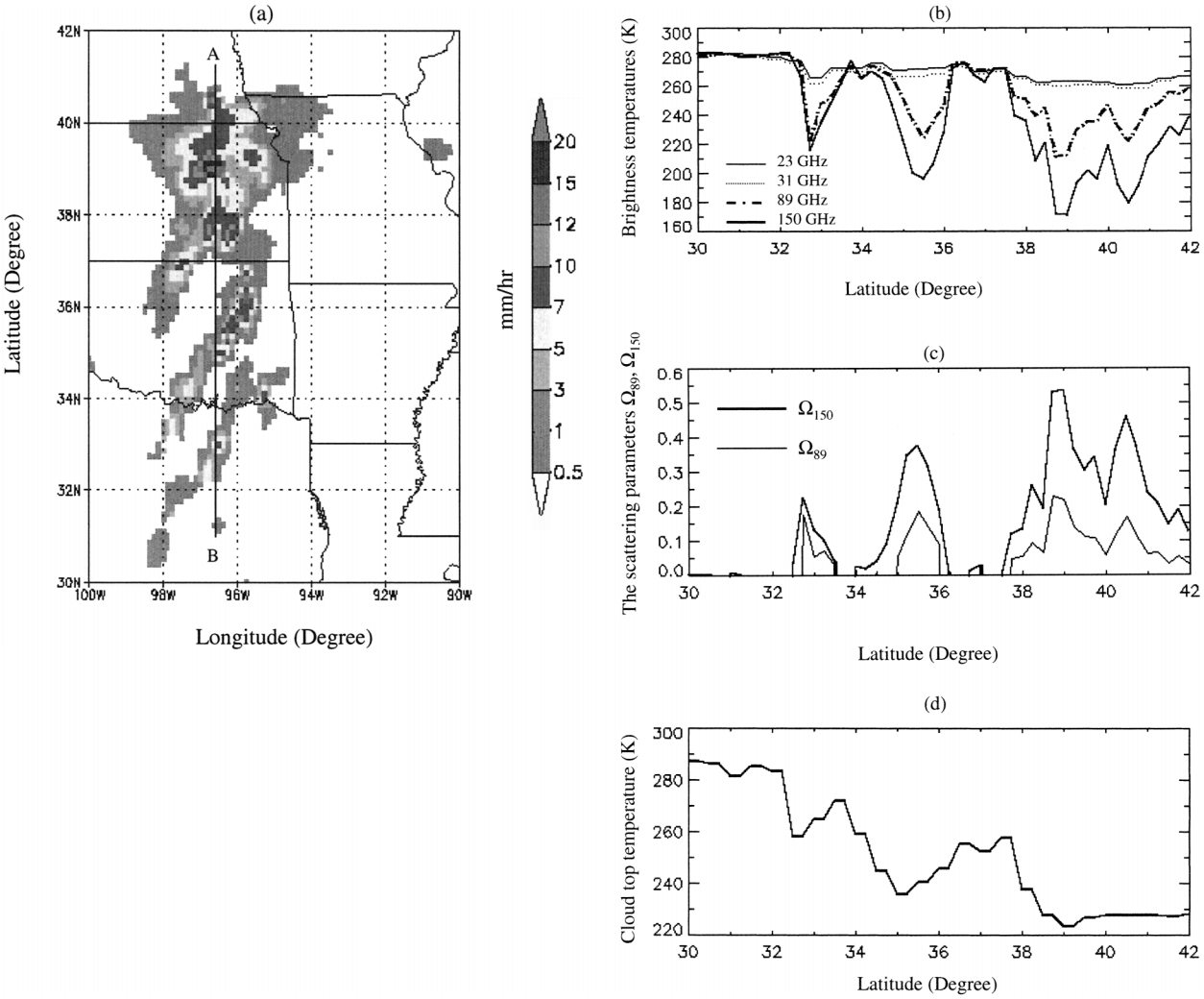

FIG. 4. (a) NCEP multisensor hourly rainfall for a winter storm that occurred on 23 Nov 1999, (b) brightness temperature depressions at the cross section of the storm, (c) the variation of scattering parameters of 89 and 150 GHz, (d) cloud-top temperatures estimated from the collocated IR 12-μm measurements, (e) cloud ice water path, and (f) ice particle effective diameter.

caused by the time difference between the satellite measurements and NCEP rainfall data. In particular, the retrieved IWP represents an instantaneous observation, whereas NCEP rainfall data are a cumulative estimate during an hour period.

b. Tropical cyclone

The relationship between IWP and other atmospheric properties such as cloud liquid water, precipitable water, and cloud-top temperature are examined over an oceanic cyclone system, as shown in Figs. 5a–c. All images illustrate some interesting features such as spiral rainbands associated with larger IWP and particle size. In particular, Fig. 5d depicts the retrieved IWP against cloud-top temperature. Note that IWP and cloud-top temperature are correlated well, especially for precipitation clouds with cloud-top temperature colder than -40°C. Large IWP values correspond to colder cloud-top temperature, which is a typical feature of convective precipitating systems. This result is also similar to that found in the previous studies for nonraining cirrus clouds (Liu and Curry 1999; Heymsfield and Platt 1984).

c. Global retrieval

The retrieval algorithm, including the screening method, is applied for AMSU data on a global scale. Figure 6 shows a global distribution of retrieved IWP, which is a monthly composite using AMSU data from morning orbits in April of 2000. The ice clouds are depicted over both land and ocean and exhibit a continuous transition across coastlines. Cloud ice water is relatively high within the intertropical convergence zone (ITCZ). Over the eastern Pacific, double ITCZ cloud bands are shown,

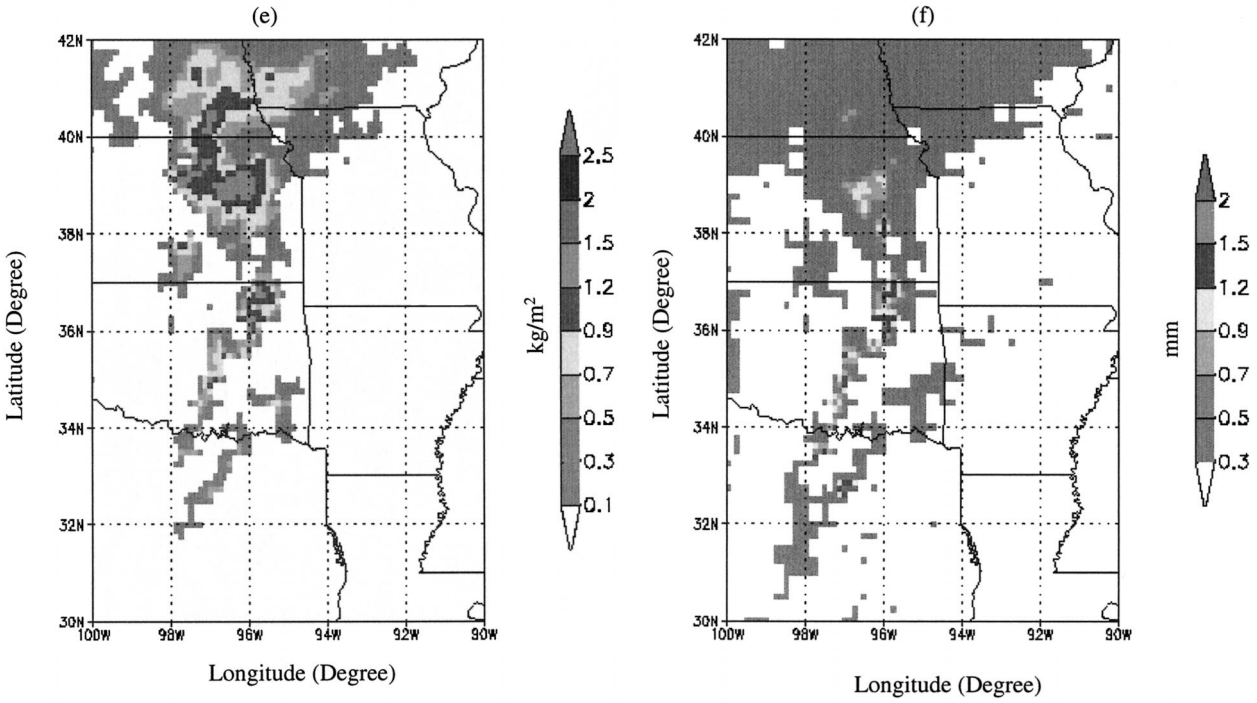

FIG. 4. (*Continued*)

which is a typical rainfall structure during this season. Over the central Indian Ocean, the ice clouds also prevail and may be associated with deep convection upstream further east. Note that some possible false signals are still left over the Tibetan Plateau, which may be caused by the cold surface temperature.

5. Error analysis

Several major sources of errors in retrieving cloud ice water path result from the uncertainties in the scattering parameters, bulk volume density, and effective particle diameter. The retrieval error of particle effective diameter is also directly dependent on the uncertainties in scattering parameters and bulk volume density, as discussed below.

a. Errors in retrieved effective diameter

As shown in Eq. (11), the ice particle effective size is nonlinearly proportional to the scattering parameter ratio. The regression coefficients are also slightly dependent on the bulk volume density. The percent of errors in the diameter can be derived from Eq. (11) as follows:

$$\frac{\Delta D_e}{D_e} = g_1(D_e, r, \rho_i)\frac{\Delta r}{r} + g_2(D_e, r, \rho_i)\frac{\Delta \rho_i}{\rho_i}, \quad (15)$$

with

$$\frac{\Delta r}{r} = h_1(T_{B0}, T_B) \times \left(\frac{\Delta T_{B0}}{T_{B0}} - \frac{\Delta T_B}{T_B}\right), \quad (16)$$

where T_{B0} and T_B are the upwelling brightness temperatures at ice cloud base and top, respectively, and h_1 is a nonlinear amplifying factor that is modulated by the scattering intensity of ice particles. Note that the cloud-base temperature is one of the major error sources in estimating the scattering parameter ratio. Figure 7a displays retrieved D_e error against the error in estimating the cloud-base brightness temperature. The error apparently increases linearly as the error of cloud-base brightness temperature increases. The effect of cloud-base temperature error on the D_e retrieval is less significant for the larger ice particles. A 4.0-K error of the cloud-base temperatures results in a 5% retrieval error for D_e larger than 2.0 mm. The D_e retrieval error resulting from AMSU instrument noises (2 K) is less than 1%.

The second term of Eq. (15) represents the retrieval error due to the uncertainty in the particle bulk volume density used. As shown in Fig. 7b, for smaller D_e($<$1.0 mm), the D_e error is less sensitive to the density error and is normally less than 5%. For a given error in the density, however, the retrieved D_e contains much larger errors at large sizes.

Note that Eqs. (11) and (12) are derived using an exponent of 2 in the particle size distribution, which is a gamma function. Here, we also test the effect of the exponent on IWP and D_e retrieval using three different values from 1 to 3. It is found that the retrieval of D_e

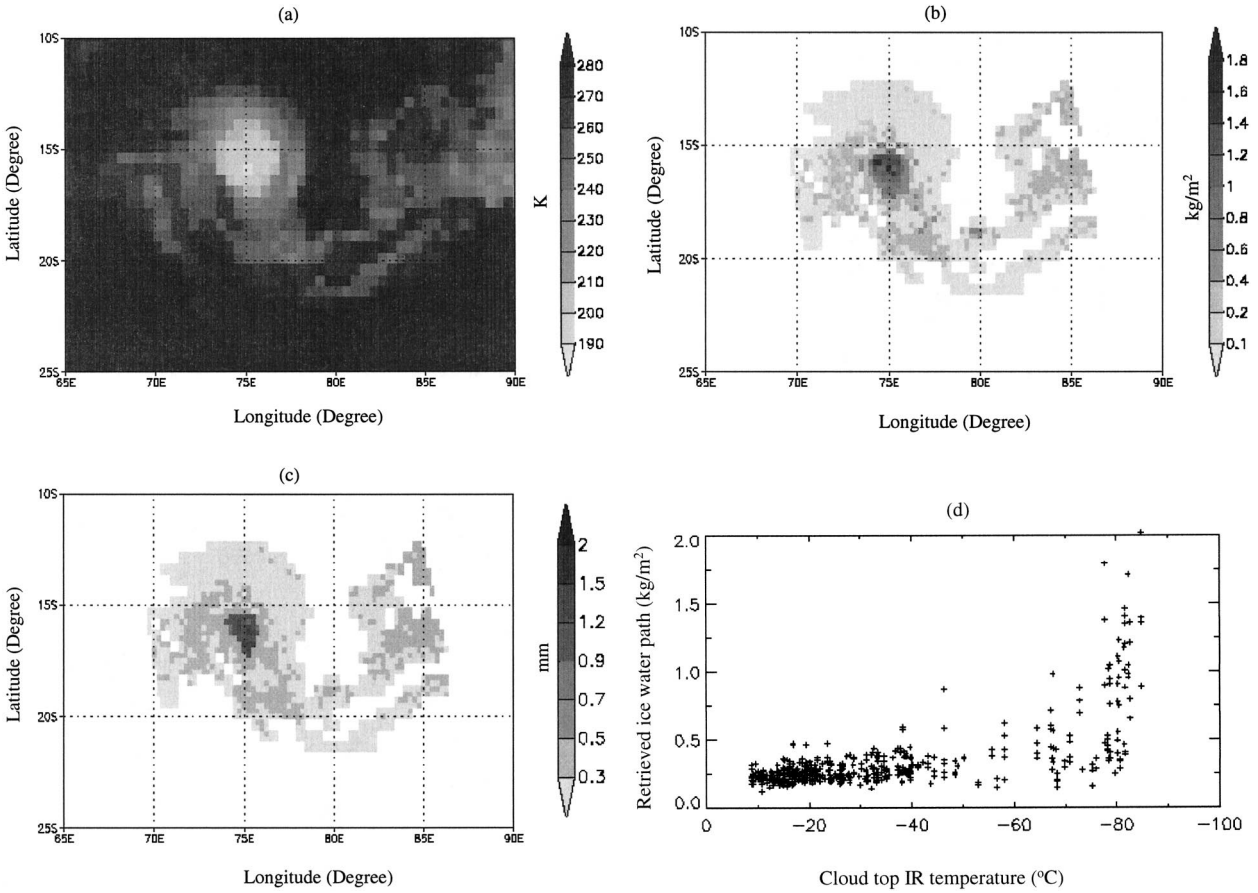

FIG. 5. (a) IR temperature measurements for a tropical cyclone system that occurred on 28 Feb 2000, (b) retrieved cloud ice water path, (c) ice particle effective diameter, and (d) cloud ice water vs cloud-top temperature.

is not sensitive to this parameter. In general, the error is less than 2%.

b. Errors in retrieved cloud ice water path

As shown in Eq. (9), IWP is a function of ice particle effective diameter, the bulk volume density, and the scattering parameter. Its retrieval error is derived as follows:

$$\frac{\Delta \mathrm{IWP}}{\mathrm{IWP}} = \frac{\Delta \Omega}{\Omega} + f_1(D_e, \rho_i)\frac{\Delta D_e}{D_e} + f_2(D_e, \rho_i)\frac{\Delta \rho_i}{\rho}, \quad (17)$$

where

$$\frac{\Delta \Omega}{\Omega} = \frac{T_{B0}}{T_{B0} - T_B}\left(\frac{\Delta T_{B0}}{T_{B0}} - \frac{\Delta T_B}{T_B}\right). \quad (18)$$

From Eq. (17), the IWP error is linearly related to the error of the scattering parameter but nonlinearly to the uncertainties in diameter and bulk density because the relationship between Ω_N and D_e is nonlinear and depends on the particular ice particle size distribution and bulk volume density.

As shown in Eq. (18), two major error sources result in the errors in scattering parameters. These include the errors in estimating cloud-base temperature and errors caused by instrument noise. For AMSU, the instrument noise is generally 2 K. This alone could introduce 3%–10% of the errors in Ω for the brightness temperature depression ranging from 120 to 20 K.

Figure 8a shows the IWP error as a function of the error of the cloud-base brightness temperature. A 10-K error of the cloud-base temperature could result in 10% retrieval error with a 60-K brightness temperature depression at 150 GHz. The second term in Eq. (17) represents the IWP error due to the uncertainty in the ice particle size. As shown in Fig. 8b, the IWP error is directly proportional to the error of particle size. This can be also explained with the result in Fig. 1. For a small particle size ($<$0.5 mm), Ω_N changes very rapidly with D_e. Thus, a small error in D_e would result a large error in Ω_N or IWP. As D_e increases, Ω_N changes slowly with D_e and is less sensitive to the error in D_e. For 20% of D_e error, which is highly possible from the analysis in section 5a, the error of IWP ranges from 10% to 20% for the particle size between 1.0 and 2.5 mm (see Fig. 8b).

The third term of Eq. (17) is the retrieval error due

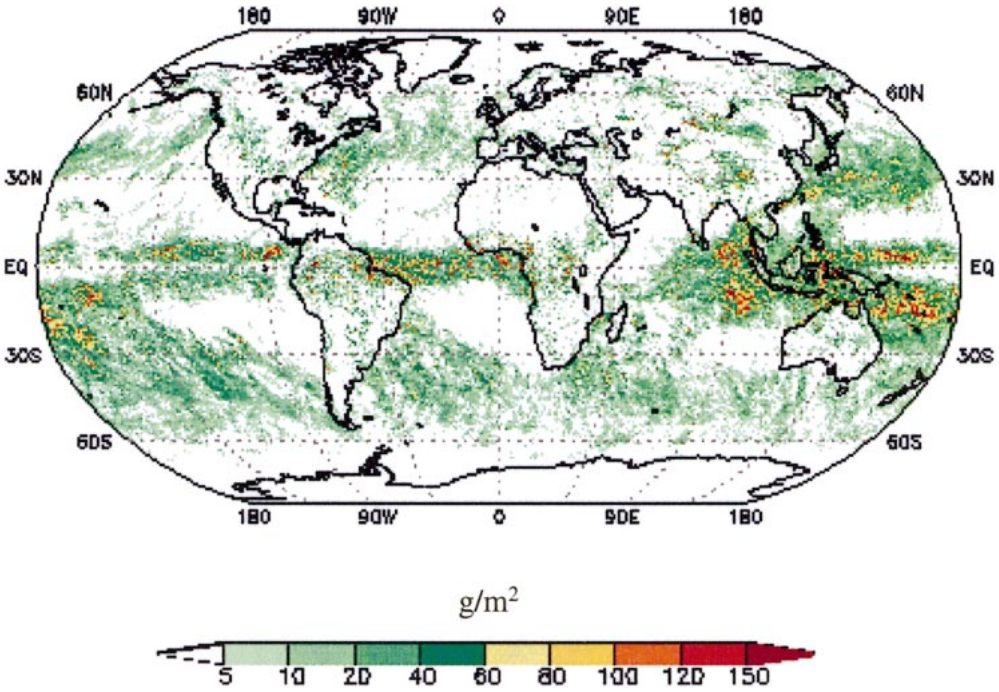

FIG. 6. Monthly mean IWP derived from AMSU in Apr 2000.

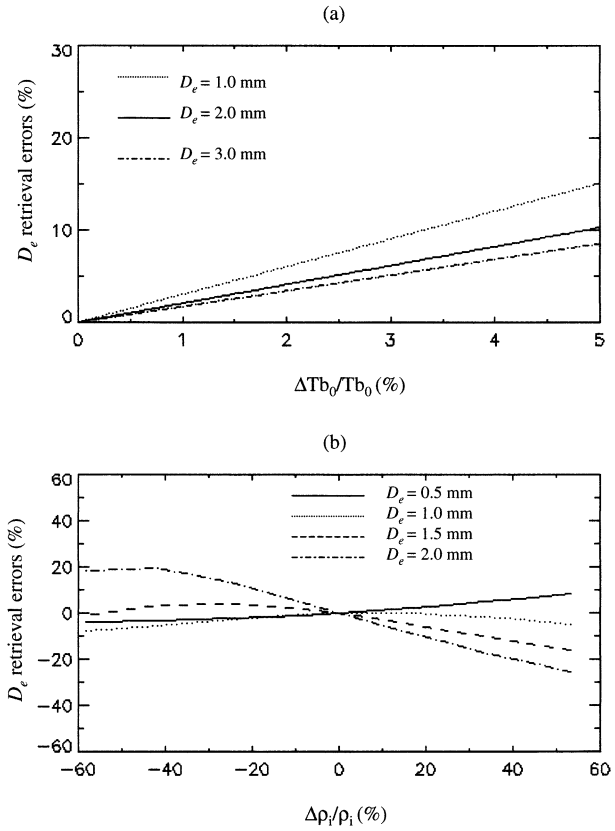

FIG. 7. The error of retrieved particle effective diameter due to (a) the error in estimating cloud-base brightness temperature and (b) the error in particle bulk volume density.

to the uncertainties in the particle bulk density. As shown in Fig. 8c, IWP error increases as the ice particle bulk density varies from its true value. The error characteristics are also modified slightly by the particle effective size. For a 30% uncertainty, the IWP error is about 25%. In addition, there is about a 5% IWP retrieval error from the uncertainty on the shape parameter γ of the gamma size distribution.

6. Summary and conclusions

A new algorithm is developed to retrieve the ice water path and particle size from the AMSU measurements at 89 and 150 GHz. Both IWP and D_e are related to the ice particle scattering parameters, which are determined from the upwelling brightness temperatures at ice cloud tops and bases. The ratio of the scattering parameters measured at two frequencies provides a direct estimate of D_e for the particles near millimeter size. The relationships between ice scattering parameters and ice particle effective diameters (e.g., D_e–r and Ω_N–D_e) are derived using a modified gamma size distribution. IWP is proportional to the particle effective diameter and ice scattering parameter with a given ice particle bulk volume density. The upwelling brightness temperatures at ice cloud bases at 89 and 150 GHz are estimated using the AMSU lower-frequency measurements at 23 and 31 GHz. A screening procedure is also developed to remove the false scattering signatures due to various surface materials.

Several major sources of errors are identified and an-

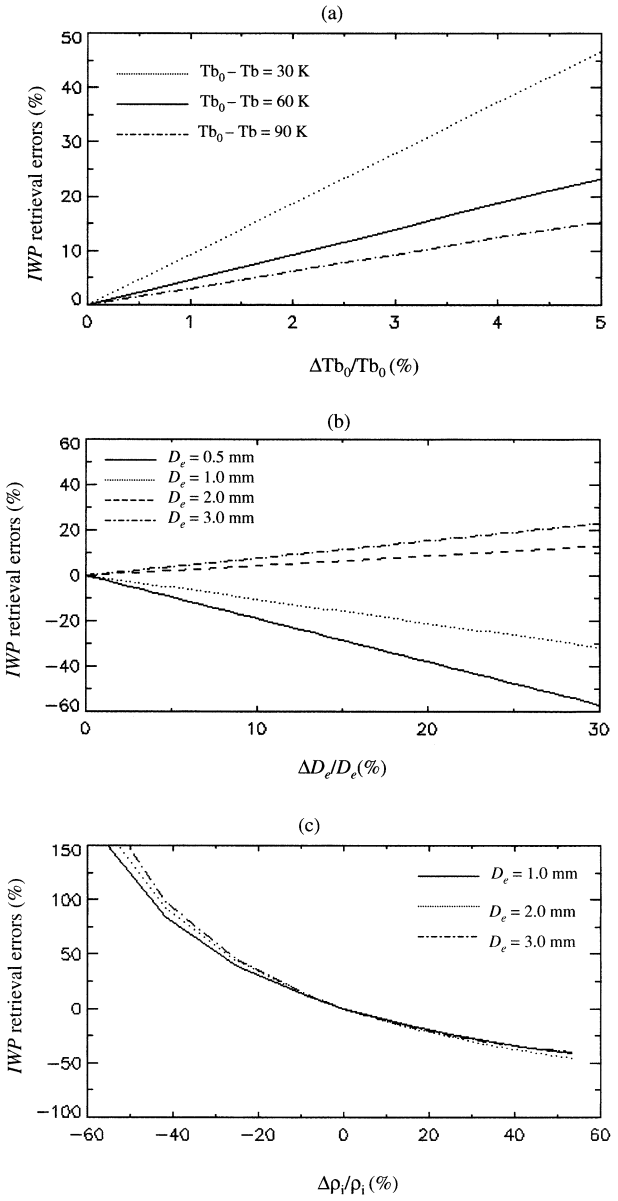

FIG. 8. The error of retrieved ice water path due to (a) the error in estimating cloud-base brightness temperature, (b) the error in retrieved diameter, and (c) the error in particle bulk volume density.

alyzed. It is shown that the D_e errors are primarily caused by the uncertainty of the particle bulk volume density and the errors in estimating cloud-base brightness temperatures. For a 3% cloud-base temperature error, the D_e error is about 10%. For a 30% uncertainty in bulk density, the D_e error ranges from 5% to 20%, depending on D_e. It is found that D_e retrieval is not sensitive to the exponent parameter in the size distribution.

The error sources for IWP are associated with the cloud-base brightness temperature and the density. The errors in retrieved D_e result in an additional error in IWP. In particular, a 10-K error in cloud-base temperature results in 10% IWP error when the brightness temperature depression is 60 K at 150 GHz. For a given error in cloud-base temperature, however, the retrieved IWP contains much larger errors for ice clouds, producing less brightness temperature depression at 89 GHz. The uncertainty in the ice particle bulk volume density contributes the most to the IWP retrieval error. IWP is underestimated as the ice particle bulk density becomes positively biased. For a 30% error in the density, the IWP error is up to 50%, depending on ice particle types. A 20% error in the retrieved D_e would result in a 10%–20% error in the retrieved IWP for ice particle size between 1.0 and 2.5 mm. There is about 3%–10% error in IWP due to the instrument noises (± 2 K) for the satellite-measured brightness temperature depression ranging from 120 to 20 K. Uncertainty in the exponent parameter in the size distribution results in about 5% error in the retrieved IWP.

The algorithm is examined under various weather conditions, and the resulting distributions of IWP and D_e are compared with cloud liquid water, cloud-top temperatures, and surface rainfall. It was found that the algorithm works reasonably well in depicting precipitating ice clouds. For a cloud system near the coast, the retrieved ice cloud water path exhibits a continuous transition. The algorithm apparently does not detect the thin cirrus clouds surrounding the precipitating areas because of a lack of sensitivity at 89 GHz. These thin clouds may be detected using even-higher frequencies (e.g., 150 and 220 GHz) or visible-wavelength measurements.

Acknowledgments. The authors thank three anonymous reviewers for their valuable suggestions. Thanks also go to Ralph Ferraro and Norm Grody for their valuable discussions during the research and to Huan Meng for her help in implementing the algorithm to the NOAA operational system. This work is funded by the NOAA/NESDIS/Office of System Development.

REFERENCES

Adler, R. F., A. J. Negri, P. R. Keehn, and I. M. Hakkarinen, 1993: Estimation of monthly rainfall over Japan and surrounding waters from a combination of low-orbit microwave and geosynchronous IR data. *J. Appl. Meteor.*, **32,** 335–356.

Cumming, W. A., 1952: The dielectric properties of ice and snow at 3.2 centimeters. *J. Appl. Phys.*, **23,** 768–773.

Deeter, M. N., and K. F. Evans, 2000: A novel ice-cloud retrieval algorithm based on the Millimeter-Wave Imaging Radiometer (MIR) 150- and 220-GHz channels. *J. Appl. Meteor.*, **39,** 623–633.

Ebert, E. E., and J. A. Curry, 1992: A parameterization of ice cloud optical properties for climate models. *J. Geophys. Res.*, **97,** 970–978.

Evans, F. K., and G. L. Stephens, 1995a: Microwave radiative transfer through clouds composed of realistically shaped ice crystals. Part I: Single scattering properties. *J. Atmos. Sci.*, **52,** 2041–2057.

——, and ——, 1995b: Microwave radiative transfer through clouds composed of realistically shaped ice crystals. Part II: remote sensing of ice clouds. *J. Atmos. Sci.*, **52,** 2058–2072.

——, S. J. Walter, A. J. Heymsfield, and M. N. Deeter, 1998: Modeling of submillimeter passive remote sensing of cirrus clouds. *J. Appl. Meteor.*, **37,** 184–205.

Fu, Q., and K. N. Liou, 1993: Parameterization of the radiative properties of cirrus clouds. *J. Atmos. Sci.,* **50,** 2008–2025.

Grody, N. C., 1991: Classification of snow cover and precipitation using the Special Sensor Microwave/Imager (SSM/I). *J. Geophys. Res.,* **96,** 7423–7435.

——, J. Zhao, R. Ferraro, F. Weng, and R. Boers, 2001: Determination of precipitable water and cloud liquid water over oceans from the *NOAA-15* advanced microwave sounding unit. *J. Geophys. Res.,* **106,** 2943–2954.

Heymsfield, A. J., and C. M. R. Platt, 1984: A parameterization of the particle size spectrum of ice clouds in terms of the ambient temperature and the ice water content. *J. Atmos. Sci.,* **41,** 846–855.

——, and L. J. Donner, 1990: A scheme for parameterization ice cloud water in general circulation models. *J. Atmos. Sci.,* **47,** 1865–1877.

Holinger, J. P., 1971: Passive microwave measurements of sea surface roughness. *IEEE Trans Geosci. Elec.,* **9GE,** 165–169.

Klein, L. A., and C. T. Swift, 1977: Emissivity for calm water. *IEEE Trans. Antennas Propag.,* **25,** 104–111.

Liou, K.-N., 1986: Influence of cirrus clouds on weather and climate processes: A global perspective. *Mon. Wea. Rev.,* **114,** 1167–1199.

Liu, G., and J. A. Curry, 1998: Remote sensing of ice water characteristics in tropical clouds using aircraft microwave measurements. *J. Appl. Meteor.,* **37,** 337–355.

——, and ——, 1999: Tropical ice water amount and its relations to other atmospheric hydrological parameters as inferred from satellite data. *J. Appl. Meteor.,* **38,** 1182–1194.

——, and ——, 2000: Determination of ice water path and mass median particle size using multichannel microwave measurements. *J. Appl. Meteor.,* **39,** 1318–1329.

Minnis, P., K.-N. Liou, and Y. Takano, 1993: Inference of cirrus cloud properties from satellite-observed visible and infrared radiances. Part I: Parameterization of radiance fields. *J. Atmos. Sci.,* **50,** 1279–1304.

Rossow, G. W., and R. A. Schiffer, 1991: ISCCP cloud data products. *Bull. Amer. Meteor. Soc.,* **72,** 2–20.

Seo, D. J., 1998: Optimal estimation of rainfall fields using radar rainfall and rain gauge data. *J. Hydrology,* **208,** 37–52.

Spencer, R. W., S. Olson, W. Rongzhong, D. W. Martin, J. A. Weinman, and D. A. Santek, 1983: Heavy thunderstorms observed over land by the *Nimbus-7* Scanning Multichannel Microwave Radiometer. *J. Appl. Meteor.,* **22,** 1041–1046.

Stephens, G. L., and P. J. Webster, 1981: Clouds and climate: Sensitivity of simple systems. *J. Atmos. Soc.,* **104,** 677–690.

Stogryn, A., 1972: A study of radiometric emission from a rough sea surface. NASA Contractor Rep. CR-2088.

Stowe, L. L., P. A. Davis, and E. P. McClain, 1999: Scientific basis and initial evaluation of the CLAVR-1 global clear/cloud classification algorithm for the advanced very high resolution radiometer. *J. Atmos. Oceanic Technol.,* **16,** 656–681.

Ulbrich, C. W., 1983: Natural variations in the analytical form of the raindrop size distribution. *J. Climate Appl. Meteor.,* **22,** 1764–1775.

Vivekanandan, J., J. Turk, and V. N. Bringi, 1991: Ice water path estimation and characterization using possible microwave radiometry. *J. Appl. Meteor.,* **30,** 1407–1421.

Wang, J. R., J. Zhan, and P. Pacette, 1997: Storm-associated microwave radiometric signatures in the frequency range of 90–220 GHz. *J. Atmos. Oceanic Technol.,* **14,** 13–31.

Weng, F., 1992: A multi-layer discrete-ordinate method for vector radiative transfer in a vertically-inhomogeneous, emitting and scattering atmosphere. Part I: Theory. *J. Quant. Spec. Radiat. Trans.,* **47,** 19–33.

——, and N. C. Grody, 1998: Physical retrieval of land surface temperature using the special sensor microwave imager. *J. Geophys. Res.,* **103,** 8839–8848.

——, and ——, 2000: Retrieval of ice cloud parameters using a microwave imaging radiometer. *J. Atmos. Sci.,* **57,** 1069–1081.

——, R. R. Ferraro, and N. C. Grody, 2000: Effects of AMSU cross-scan asymmetry of brightness temperatures on retrieval of atmospheric and surface parameters. *Microwave Radiometry and Remote Sensing of the Earth's Surface and Atmosphere,* P. Pampaloni and S. Paloscia, Eds., VSP, 255–262.

——, B. Yan, and N. C. Grody, 2001: A microwave land emissivity model. *J. Geophys. Res.,* **106,** 20 115–20 123.